









Effect of Post-thermal Annealing on the Structural, Morphological, and Optical Properties of RF-sputtered In₂S₃ Thin Films

Neslihan AKCAY^{1,2*} , Berkcan ERENLER¹ , Yunus OZEN^{1,3} , Valery Feliksovich GREMENOK⁴ ,
Konstantin Pavlovich BUSKIS⁴ , Suleyman OZCELIK^{1,5} 

¹Photonics Application & Research Centre, Gazi University, 06500, Ankara, Turkey

²Department of Mechanical Engineering, Faculty of Engineering, Baskent University, 06790, Ankara, Turkey

³Department of Physics, Faculty of Science, Gazi University, 06500, Ankara, Turkey

⁴State Scientific and Production Association «Scientific-Practical Materials Research Centre of the National Academy of Sciences of Belarus», 220072, Minsk, Belarus

⁵Department of Photonics, Faculty of Applied Sciences, Gazi University, 06500, Ankara, Turkey

Highlights

- In₂S₃ films were deposited on SLG substrates by RF sputtering technique at 150 °C.
- The thermal annealing treatment at 450 °C improved the crystallization and morphology of the films.
- The films exhibited slightly sulfur deficit composition.
- PL spectra showed broad emission bands at ~ 1.70, 2.20 and 2.71 eV corresponding different defects.

Article Info

Received: 24 Feb 2022

Accepted: 17 July 2022

Keywords

In₂S₃
indium sulfide
Cd-free buffer layers
Sputtering
Thermal annealing

Abstract

Indium sulfide films were deposited by radio frequency magnetron sputtering technique on soda lime glass substrate. The deposition was conducted at the temperature of 150 °C and prepared films were then thermally annealed under argon atmosphere at 350 °C and 450 °C for 30 min. The impact of post-thermal annealing treatment on the properties of the films was investigated. From X-ray diffraction analysis, the formation of the stable tetragonal β-In₂S₃ crystal structure was substantiated and revealed that the thermal annealing treatment at 450 °C improved the crystallization of the films. The change in surface topographies and morphologies of the films depending on the post-thermal annealing process were examined by atomic force microscopy and scanning electron microscopy techniques, respectively. The stoichiometric ratio of constituent elements in the films was obtained by elemental analysis and it was seen that the films had slightly sulfur (S) deficit composition. It was found that the concentration of S slightly increased with the thermal annealing process. The room temperature photoluminescence spectra revealed that the films included vacancies of sulfur (V_S: donor) and indium (In) (V_{In}: acceptor), indium interstitial (In_i: donor) and oxygen (O) in vacancy of sulfur (O_{Vs}: acceptor) defects with strong and broad emission bands at around 1.70, 2.20, and 2.71 eV.

1. INTRODUCTION

Second generation thin film photovoltaic (PV) technologies have been deliberated as potential alternatives to crystalline silicon (Si)-based first generation solar cells due to their minimum material usage. The most leading thin film PV technologies are based on Cu(In,Ga)S₂ (CIGS) and Cu₂ZnSnS₄ (CZTS)-based chalcogenide systems. According to the Shockley-Queisser efficiency limit, CIGS and CZTS-based solar cells are expected to have theoretical efficiency value of up to ~32% [1]. However, the reported highest power conversion efficiencies so far at laboratory scale for these technologies are 23.4% and 13.0%, respectively [2]. For this reason, the development processes of these technologies continue unceasingly in order to increase their efficiency values [3]. The researchers specifically focus on the production of the thin film PV devices, all components of which are consisted of the materials that are plentiful in the earth's crust and are non-toxic. One of the most important issues with these technologies is regarding the use of toxic

*Corresponding author, e-mail: neslihanakcay@baskent.edu.tr

cadmium sulfide (CdS) buffer layer in their heterojunction device structure [4-7]. It is well known that the high-efficient devices of the CIGS and CZTS-based solar cells generally contain n-type CdS buffers which are prepared by chemical bath deposition method (CBD) [8-10]. However, liquid waste resulting from CBD method contains toxic Cd, S and ammonia and it creates environmental problems and hazards for human health [11, 12]. Therefore, there has been a great effort to replace CdS buffer by other cadmium-free materials. In addition, replacement of CdS with another material having a larger band gap than that of CdS has also a great importance in this avenue of research, particularly to increase the transmission of the light in the blue wavelength region [13, 14]. In this context, n-type semiconductor indium sulfide (In_2S_3) which belongs to III-VI group of compounds is considered as a good alternative to CdS with its direct or indirect band gap values varying between 2.1-3.3 eV. In addition to this, it has a high transmittance in the visible and near infrared (NIR) spectral regions, and also structural stability and non-toxicity [15-17]. In_2S_3 tends to crystallize in three diverse crystal structures such as cubic α - In_2S_3 (defective structure), tetragonal β - In_2S_3 (defective spinel structure) and trigonal γ - In_2S_3 (layered structure) depending on the deposition conditions, in particular to the temperature [16, 18]. However, it should be noted that the tetragonal β - In_2S_3 is the most stable phase at room temperature (RT) (till to 420 °C) among these phases [16, 18].

In_2S_3 films can be prepared by different methods, including thermal evaporation [19], CBD [20], spray pyrolysis [21], atomic layer deposition (ALD) [22], electrodeposition [23] and sputtering [24, 25]. The most common methods used for the preparation of In_2S_3 buffer layers are thermal evaporation and CBD methods in the literature and high-efficient thin film PV devices were achieved by applying In_2S_3 buffer layers deposited by these two methods. Spiering et al. obtained a record efficiency of 18.2% from a CIGS device with thermally evaporated In_2S_3 buffer layer [26]. On the other hand, Kim et al. reported 12.7% efficiency for a CZTS solar cell with a double CBD- In_2S_3 /CdS emitter [27]. Moreover, Hiroi et al. reported a record efficiency of 6.3% from a CZTS-based solar cell device with a CBD- In_2S_3 buffer. However, there are only a few studies on thin film PV devices with sputtered- In_2S_3 buffer layers in the literature [17, 28-30] and all these studies were reported on CIGS-based thin film PV devices. Hariskos et al. and Soni et al. reported the efficiencies of 15.3% and 13.84% for $\text{Cu}(\text{In,Ga})\text{Se}_2$ (CIGSe) solar cell devices with sputtered In_2S_3 buffer layers, respectively [17, 30]. It is seen that the solar cell efficiency values in these studies are comparable to those of the values obtained from the solar cell devices with In_2S_3 buffer layers prepared by thermal evaporation and CBD methods. Therefore, the sputtering method can be taken into consideration as an alternative to these methods for the preparation of the CIGS and CZTS-based thin film PV devices' buffer layers. The sputtering method is a very suitable method for a continuous deposition of solar cell devices in an in-line vacuum process and it also allows to the production of good quality and uniform In_2S_3 films over large areas. In addition, it has some other advantages over thermal evaporation and CBD method. Thermal evaporation is an expensive technique because of high amount of material loss and there can be some problems regarding the homogeneity and stoichiometry of the films in this technique. When it comes to CBD method, as it is well known, it is necessary to remove the samples from the vacuum chamber after the deposition process of the absorber films for the wet CBD process of buffer layer and subsequently reintroduce the samples to the vacuum chamber for i-ZnO/Al:ZnO window layer in vacuum-based deposition techniques. Exposure of the samples to the air in this process leads to the formation of the impurities at the surface and thus interfaces which are the reasons for the decrease in the efficiency. The use of sputtering method for the preparation of buffer layer eliminates the necessity of removing the sample from vacuum chamber during the deposition process. Thus, it can be said that the sputtering method is more advantageous than the CBD method, as it eliminates both the liquid waste problem and the necessity of removing the sample from the vacuum chamber in the deposition process of the solar cells' buffer layers. However, the number of studies on the deposition of In_2S_3 films by sputtering method is limited in the literature [17, 24, 25, 29-34] and the properties of the sputtered- In_2S_3 films are still not clear. Therefore, new studies need to be done on the sputtered- In_2S_3 films and the present shortcomings on this topic in the literature should be filled. In the study of Abou-Ras et al., In_xS_y films were deposited at three different substrate temperatures: i) without any heating, ii) at 240 °C and iii) 340 °C) and the characterizations of both prepared In_xS_y films and In_xS_y /CIGS interfaces were done. It was seen that the sulfur concentration of the films and copper, gallium, indium interdiffusion between the buffer and absorber layer increased with increasing the substrate temperature [29]. On the other hand, In_2S_3 films were prepared at different RF powers (40 W, 80 W and 120 W), sputtering pressures (5 mTorr, 7.5 mTorr and 10 mTorr), substrate temperatures (300 °C, 373 °C and 473 °C) and deposition times (30 min, 60 min and 90 min) by Wang et

al. and the structural, morphological, and optical properties of the films were examined depending on the deposition parameters [31]. In the study reported by Hwang et al., the working pressure and the substrate temperature was fixed at 3×10^{-3} Torr and 100 °C during the deposition process of In_2S_3 films, but the sputtering power were changed from 60 W to 120 W and the effect of different sputtering powers were investigated [32]. Ji et al. studied the effect of thickness on the structural, morphological, optical, and photoconductive properties of the In_2S_3 films prepared at 100 W RF power and 350 °C by RF magnetron sputtering technique [25]. In another study reported by Karthikeyan et al, In_2S_3 films were deposited at different substrates temperatures (without any heating, at 100 °C, 150 °C, 200 °C, and 250 °C) at 25 W by pulse direct current magnetron sputtering technique and they achieved to grow a single phase $\beta\text{-In}_2\text{S}_3$ without substrate heating or annealing for the first time [24]. They observed that increase in substrate temperature led to a decrease in sulfur content. In the study of Soni et al., the deposition of In_2S_3 buffer layers were performed at different sputtering powers and working pressures on CIGSe absorber layer and fabricated CIGSe solar cells were exposed to heat treatment at 210 °C for 15 minutes. They investigated sputter induced damage on the absorber layer and the effect of sputtering and annealing at the buffer layer/absorber layer interface [17]. Hariskos et al. studied the influence of the substrate temperature during the deposition of In_xS_y layer on the buffer layer/absorber layer interface formation and the solar cell performance. The substrate temperature was increased from RT to 240 °C and the highest efficiency values were obtained at around 200 °C [30]. In other two studies reported by Siol et al. and Soni et al., reactive sputtering method was used to prepare In_2S_3 films unlike the other studies [33, 34]. In the study of Siol et al., the deposition of the films was performed at 40 W sputtering power and CZTS solar cell devices were fabricated to show the feasibility of sputtered In_2S_3 buffer layers in CZTS solar cell device [33]. Soni et al. reported that the deposition of buffer layer at slower sputtering rates with H_2S reactive gas enhanced the interface quality and uniformity [34].

In these previously reported studies, it has been revealed that the deposition parameters such as sputtering power, working pressure and deposition temperature have a great effect on the film composition, structural, morphological, and optical properties in magnetron sputtering method. Particularly, the sputtering power, working pressure and deposition temperature are much more effective on the composition of the films due to the large difference in vapor pressures of the In and S elements during sputtering process. Therefore, the deposited films may have a non-stoichiometric composition, or the uniformity of the films may change depending on the sputtering power, working pressure and deposition temperature. Another important issue is the possibility of high temperature and high sputtering power induced damage on the absorber layer during the deposition process. In this context, we preferred to conduct the deposition of the films at lower temperatures and at lower sputtering powers with the aim of reducing this possible damage on the absorber layer. In our study, the In_2S_3 films were deposited at a temperature of 150 °C by applying a 20 W RF power, and subsequently, a post thermal annealing process was applied to as-deposited films at the temperatures of 350 °C and 450 °C under argon (Ar) atmosphere in a tube furnace, outside the deposition chamber unlike the existing studies in the literature. As a result of our literature review, we concluded that a lot of work has been done on thermal annealing of In_2S_3 films in the literature [19, 35-39]. However, as we mentioned above, in all these studies, the films were deposited by mostly thermal evaporation and CBD methods. When it comes to the abovementioned studies where In_2S_3 films were grown by magnetron sputtering technique [17, 24, 25, 29-34], it was seen that the In_2S_3 films were deposited at different substrate temperatures, but no thermal annealing process was applied to the films after the deposition process. To the best of our knowledge, such thermal annealing has not been done before in the literature on In_2S_3 films deposited by magnetron sputtering technique.

In the present research, the effect of post-thermal annealing process on the physical properties of RF-sputtered In_2S_3 films at low sputtering power were scrutinized by utilizing a variety of characterization techniques. In our study, the structural and morphological characterizations showed that the annealing treatment at the temperature of 450 °C improved the crystallization and surface morphology of the films. Herein we concluded that the films with a thickness of about 280 nm annealed at 450 °C were suitable for use as buffer layers in thin film PV applications. However, within the scope of more detailed studies, the physical properties of the films might be enhanced through optimizing the thickness of the films for the thin film solar cell applications.

2. EXPERIMENTAL

In₂S₃ films were prepared on soda lime glass (SLG) by using RF magnetron sputtering method in a confocal, Nanovak, NVTS500, magnetron sputtering system. A stoichiometric ceramic In₂S₃ target (In:S=40:60 at%) with a 99.95% purity (2" dia × 0.125" thick) was used as a sputtering source for the depositions. Target-to-substrate holder distance was kept at 12 cm with an angle of 45°. The homogeneity of the films was achieved by rotating the substrate holder at 5 rpm. After loading the substrates to the deposition system, it was evacuated to a base pressure of ~10⁻⁷ Torr and then Ar with a purity of 99.995% as a sputtering gas was introduced to the chamber. Prior to the deposition process, the target was pre-sputtered at 20 W for 8 min to remove contaminations and oxides over its surface. The working pressure was kept at 20 mTorr during the deposition. All depositions were performed using a sputtering power of 30 W for 30 min at a substrate temperature of 150 °C. The as-deposited film's thickness was determined as ~280 nm by profilometer measurement. The as-deposited films were subsequently thermally annealed at 350 °C and 450 °C temperatures for a period of 30 min. The annealing process was conducted under Ar atmosphere keeping the pressure at 3 mbar in one zone of a two-zoned tubular diffusion furnace. Before the thermal annealing treatment, the base pressure of the tube in the furnace was decreased to 10⁻⁴ mbar and cleaned with Ar gas. The as-deposited and thermally treated films were named as IS, IS-350 (350 °C) and IS-450 (450 °C), respectively.

The X-ray diffraction (XRD) exploration was accomplished in a APD 2000 PRO X-ray diffractometer to observe crystallographic properties of the films using Cu K α radiation ($\lambda=1.54052$ Å). The elemental composition of the films was investigated by energy dispersive X-ray spectroscopy (EDX) using a Quatax 200 EDS detector (Bruker, Germany). The topographical analysis of the films was done by atomic force microscopy (AFM) technique (hpAFM, Nano-Magnetics Instruments). The surface images of the films were collected in dynamic mode scanning at RT. Surface and cross-sectional morphologies of the films were also examined by scanning electron microscope (SEM) (Hitachi S-4800 with Supra40). The photoluminescence (PL) studies were conducted by a Fluorolog-3, Horiba, Jobin-Yvon spectrofluorometer system using a He-Cd laser source with excitation wavelength of 325 nm at RT. Dektak 150 a contact mode profilometer was employed to obtain the thickness of the as-deposited films.

3. RESULTS and DISCUSSION

3.1. Structural Characterization

X-ray diffraction patterns of the as-deposited and thermally annealed In₂S₃ films were given in Figure 1. It is evident from the XRD patterns that the as-deposited film (the sample IS) exhibited low-intensity XRD peaks at $2\theta=27.59^\circ$, $2\theta=28.76^\circ$, $2\theta=33.43^\circ$ and $2\theta=48.01^\circ$ of (109), (206), (0012) and (2212) planes of the tetragonal β -In₂S₃ phase, respectively (ICDD: 25-0390). After the post-thermal annealing treatment at 350 °C, additional peaks appeared at $2\theta=14.30^\circ$, $2\theta=23.47^\circ$, $2\theta=43.81^\circ$, $2\theta=56.35^\circ$, $2\theta=59.65^\circ$, and $2\theta=66.86^\circ$ corresponding (103), (116), (1015), (3015), (4012), and (4015) planes of the tetragonal β -In₂S₃ phase, respectively (ICDD: 25-0390 and ICDD: 73-1366). When the post-thermal annealing temperature increased to 450 °C from 350 °C, the film showed an additional diffraction peak at $2\theta=36.93^\circ$ corresponding (303) plane of the tetragonal β -In₂S₃ phase. It is noteworthy to mention here that the occurrence of manifold peaks in the diffraction patterns suggest the polycrystallinity of the films and it increased with the post-thermal annealing treatment at 350 °C. As the annealing temperature increased to 450 °C from 350 °C, the intensity of the peaks got slightly stronger and sharper, and the films exhibited a preferential orientation in the (103) plane. This is an indication of an obvious enhancement in the crystallization of the films after 450 °C annealing temperature.

XRD data was used to determine some structural parameters such as lattice constants, crystallite size (D), microstrain (ϵ), dislocation density (δ), and stacking fault probability (α) for the thermally annealed films. The low intensity peaks for as-deposited film shows their poor crystalline nature, hence the structural parameters could not be calculated. Rietveld analysis [40] was used to calculate lattice constants, implemented in the «Material Analysis Using Diffraction» («MAUD») software package [41]. The lattice constants (a and c) calculated from XRD data for the samples IS-350 and IS-450 were presented in Table

1. The calculated a and c values were found to be well agreement with the standard data (ICDD: 25-0390, $a=7.619 \text{ \AA}$ and $c=32.329 \text{ \AA}$).

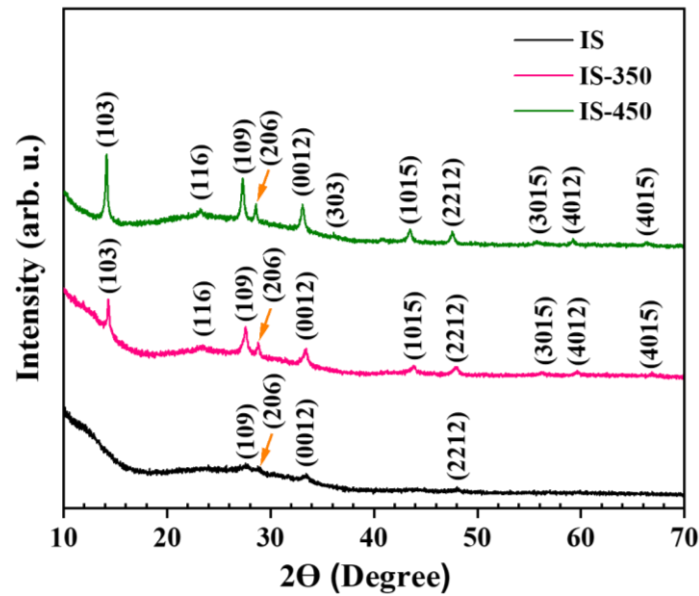


Figure 1. XRD patterns of the as-deposited and thermally annealed (at 350 °C and 450 °C) In_2S_3 films

Table 1. The Bragg angle (2θ), FWHM of the (103) and (109) peaks, and the lattice parameters of the samples IS-350 and IS-450

| Samples | | IS-350 | | IS-450 | |
|---------------------------|-----|-----------|---------|-----------|---------|
| Miller indices (hkl) | | (103) | (109) | (103) | (109) |
| Bragg angle 2θ (°) | | 14.31 | 27.57 | 14.13 | 27.30 |
| FWHM (°) | | 0.16493 | 0.30693 | 0.26815 | 0.32783 |
| Lattice constants (Å) | a | 7.585 | | 7.627 | |
| | c | 32.461 | | 32.400 | |
| Volume (Å ³) | | 1880.1176 | | 1884.3097 | |

The room-temperature powder XRD pattern and the Rietveld refinement results of In_2S_3 films were shown in Figure 2. The diffractogram of the films well matched with the pure $\beta\text{-In}_2\text{S}_3$. The good fitting parameters, the profile factor (R_p), weighted profile factor (R_{wp}), expected profile factor (R_{exp}) and goodness of fit (χ^2), suggested that the derived samples were of high quality. The average crystallite size for the films was calculated from Scherrer's formula for the intense (109) and (103) diffraction peaks [42]:

$$D = \frac{K\lambda}{\beta \cos\theta} \quad (1)$$

here K , λ , β and θ are shape factor ($K=0.9$), wavelength of the X-ray, the full width at half maximum height of the peak (FWHM) of the (109) and (103) peaks and the Bragg angle, respectively. The microstrain (ϵ) in the films was estimated by using the following relation [43]:

$$\epsilon = \frac{\beta}{4 \tan\theta} \quad (2)$$

The dislocation density (δ) was determined by Williamson and Smallman's equation [44]:

$$\delta = \frac{1}{D^2} \quad (3)$$

The existence of a stacking sequence fault in the structure lead to a shift in the peak positions observed in regard to the ideal positions of a faultless sample [45].

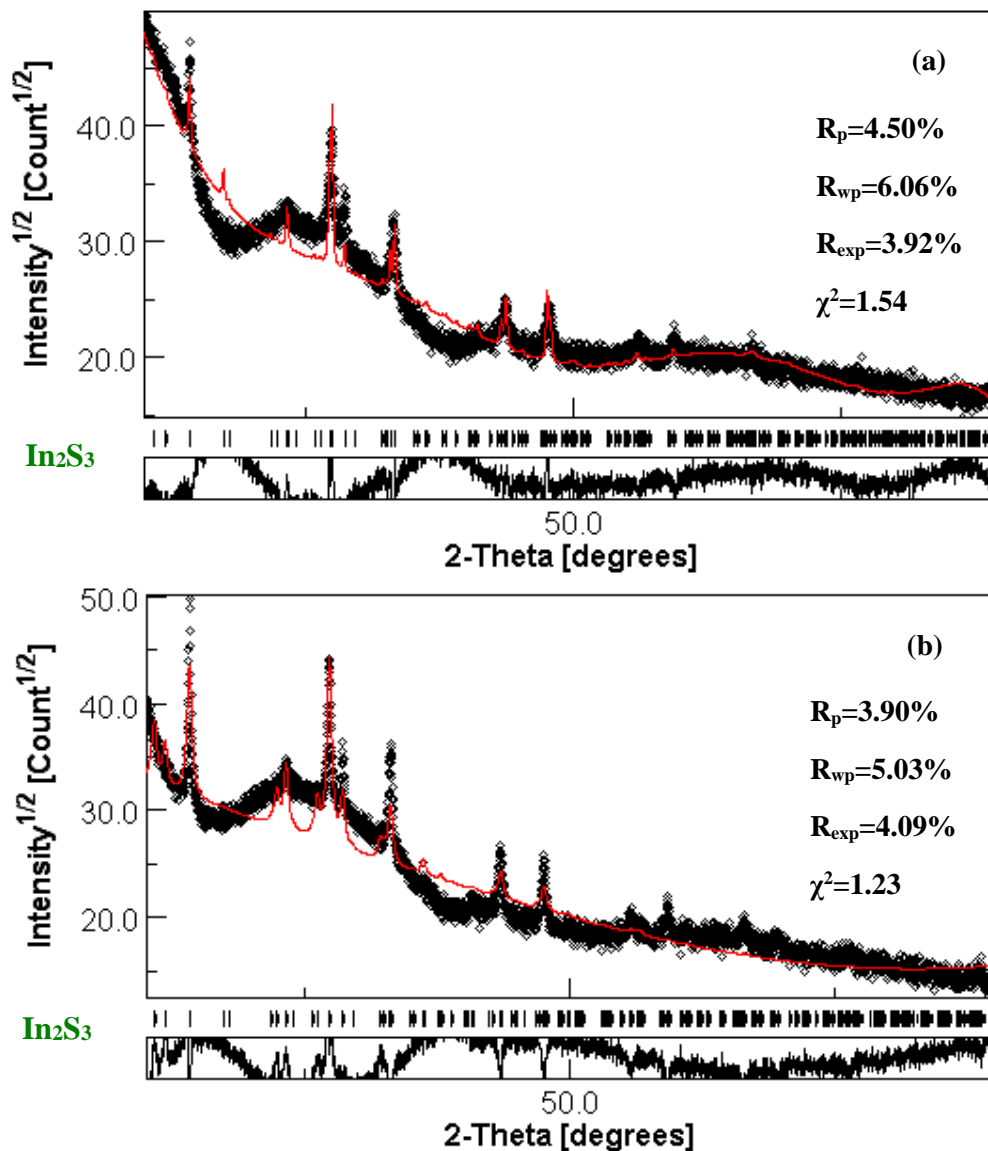


Figure 2. Rietveld refined XRD patterns of (a) the sample IS-350 and (b) IS-450 (In the patterns, the black and red curves indicate the experimental data and the results of the calculated spectrum by Rietveld method, respectively. The vertical lines show the positions of the calculated diffraction peaks, and the lower curves correspond to the difference between the experimental data and the calculated curves)

The stacking fault probabilities (α) of the samples IS-350 and IS-450 were calculated from the measured (103) and (109) peak shifts $\Delta 2\theta$ taking ICDD Card No. 25-390 as reference and using the following equation [46]:

$$\alpha = \left[\frac{2\pi^2}{45\sqrt{3}\tan\theta} \right] \Delta(2\theta) \quad (4)$$

All calculated structural parameters were given in Table 2. The average crystallite sizes were determined as 25.0 nm and 28.1 nm for the samples IS-350 and IS-450, respectively. It was observed that the crystallite size increased when the annealing temperature increased from 350 °C to 450 °C. In consistent with the results of average crystallite size, the dislocation density of the sample IS-450 was found to be slightly lower than that of the sample IS-350. The increment in crystallite size of the films tends to diminution in the grain boundaries and defect levels. The reduction in the number of defects in the sample IS-450 was also confirmed by PL analysis, which will be given in the following discussions. In addition, it was observed that there was a difference between the microstrains due to the widening of the FWHM with the effect of temperature.

Table 2. The structural parameters of the samples IS-350 and IS-450

| Samples | IS-350 | IS-450 |
|--|--------|--------|
| Miller indices (hkl) | (109) | (103) |
| Crystallite size, D (nm) (Scherrer) | 25.0 | 28.1 |
| Microstrain, ε ($\times 10^{-3}$ lines ² /m ⁴) | 5.8 | 10.0 |
| Dislocation density, δ ($\times 10^{-21}$ lines/m ²) | 1.6 | 1.3 |
| Stacking fault probability, α ($\times 10^{-3}$) | 2.91 | 3.58 |

3.2. Compositional Characterization

The elemental compositions of the samples IS, IS-350 and IS-450 were discovered through EDX and it was depicted in Figure 3.

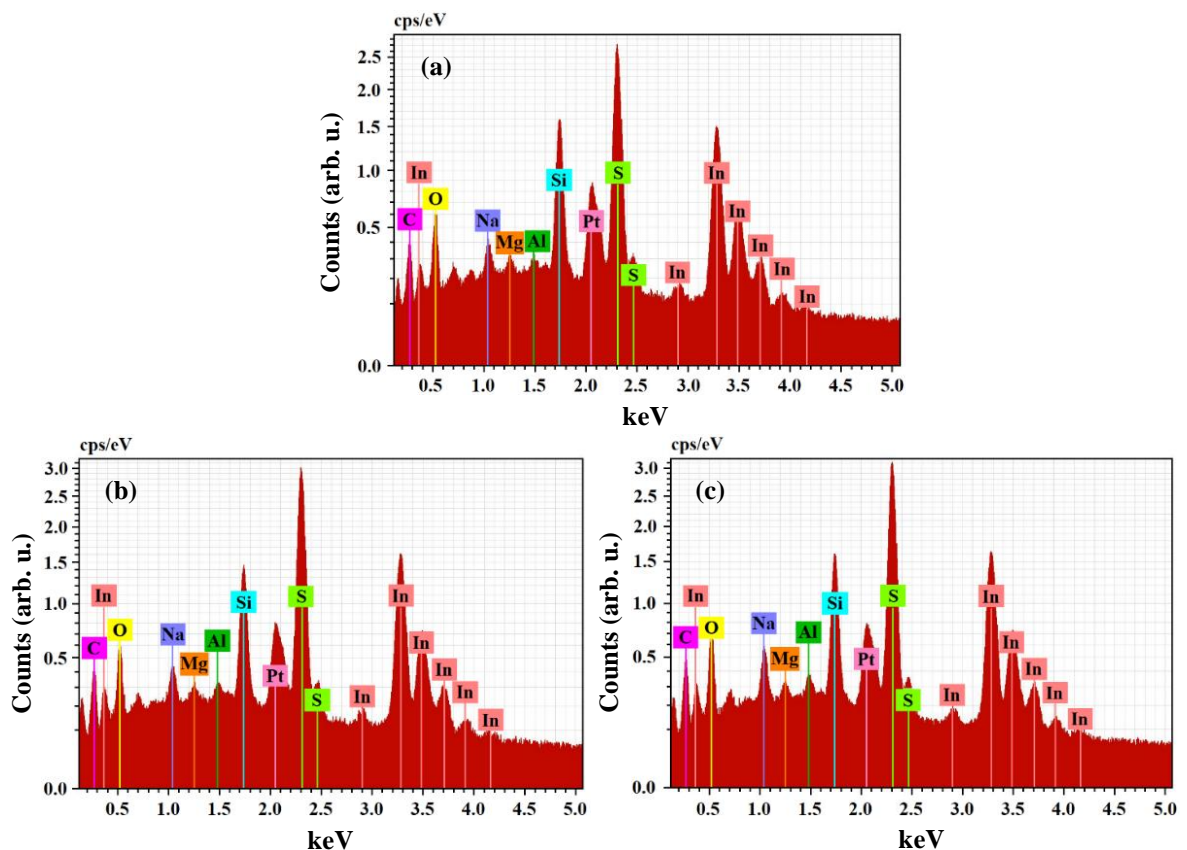


Figure 3. EDX spectra of the samples (a) IS, (b) IS-350, and (c) IS-450

The signals related to the main elements In and S constituting the films were obviously observed in the spectra. Along with the main elements in the films, the silicon (Si), oxygen (O) and sodium (Na) signals coming from SLG substrates were detected in the spectra as well. The small signals related to magnesium (Mg) and aluminum (Al) in the spectra were also associated with the constituent elements of SLG substrate. In addition, due to conductive carbon (C) tape which was used to fix the samples onto the sample holder and spraying the samples with platinum (Pt) before EDX analysis to inhibit charging problem, the peaks corresponding to the C and Pt elements were also appeared in the spectra.

Table 3 presents the atomic percentages and the atomic ratios in In_2S_3 films for the samples IS, IS-350 and IS-450. It was seen that the films were slightly sulfur deficit with atomic ratios of S/In=1.33, 1.38 and 1.38 for the samples IS, IS-350 and IS-450, respectively, considering the stoichiometric ratio of S/In=1.50. As the films have slightly sulfur deficit composition, one can consider making the post-thermal annealing process under the sulfur atmosphere by controlling the amount of sulfur. As a result, with post-thermal annealing process, no significant changes were observed in the compositions of the films.

Table 3. Elemental composition in atomic percentages (at. %) of the samples IS, IS-350 and IS-450

| Sample | Atomic percentages (at. %) | | Atomic ratios |
|--------|----------------------------|----|---------------|
| | In | S | S/In |
| IS | 43 | 57 | 1.33 |
| IS-350 | 42 | 58 | 1.38 |
| IS-450 | 42 | 58 | 1.38 |

3.3. Morphological Characterization

Figure 4 depicts 3D-AFM images of the as-deposited and thermally annealed In_2S_3 films over a scan area of $3 \mu\text{m} \times 3 \mu\text{m}$. It was obviously seen that the surface morphology of the sample IS-450 was much more uniform than those of the other samples. The sample IS-450 also exhibited the most uniform grain distribution among the samples. These results are consistent with better crystallinity of the sample IS-450 obtained in XRD results.

The average roughness (R_a), root mean square roughness (R_{rms}) and total amplitude roughness (R_t) (or called peak to valley height) values of the films estimated by AFM analysis were tabulated in Table 4. Each roughness parameter which was calculated to assess the roughness of the film surface is defined in a different way. R_a is the average deviation of the peaks and valleys from a reference line/plane on the entire measured length/area. R_{rms} is another roughness parameter which is similar to R_a , but it describes the root of square amplitude of surface roughness, and thus, it is more sensitive to peaks and valleys and their large deviations with regard to reference line/plane than R_a . As for R_t , it separates the highest peak and lowest valley in the evaluated length/area, that is, it is the vertical distance between the highest peak and lowest valley and represents the overall roughness of the surface. The R_a , R_{rms} and R_t values of the films except for the sample IS increased with increase in thermal annealing temperature. In addition, some spike-like clusters appeared on the surface of the as-deposited film. It should be stated that these large clusters are the reason for this sample to exhibit high R_a , R_{rms} and R_t values. Such clusters were not observed on the thermally annealed films' surfaces. Similar clusters on the In_2S_3 films' surfaces were reported by Kumar and et al. [47]. In this study, these kinds of clusters were identified as oxide crystallites and attributed to recrystallization in the films. However, we think that these clusters can also be associated with non-homogeneous surfaces. Moreover, the grain size increased with thermal annealing treatment for all films. This can be explained by the fact that ad-atoms combine with neighboring atoms with sufficient energy provided by the thermal annealing process at high temperatures and form larger grains.

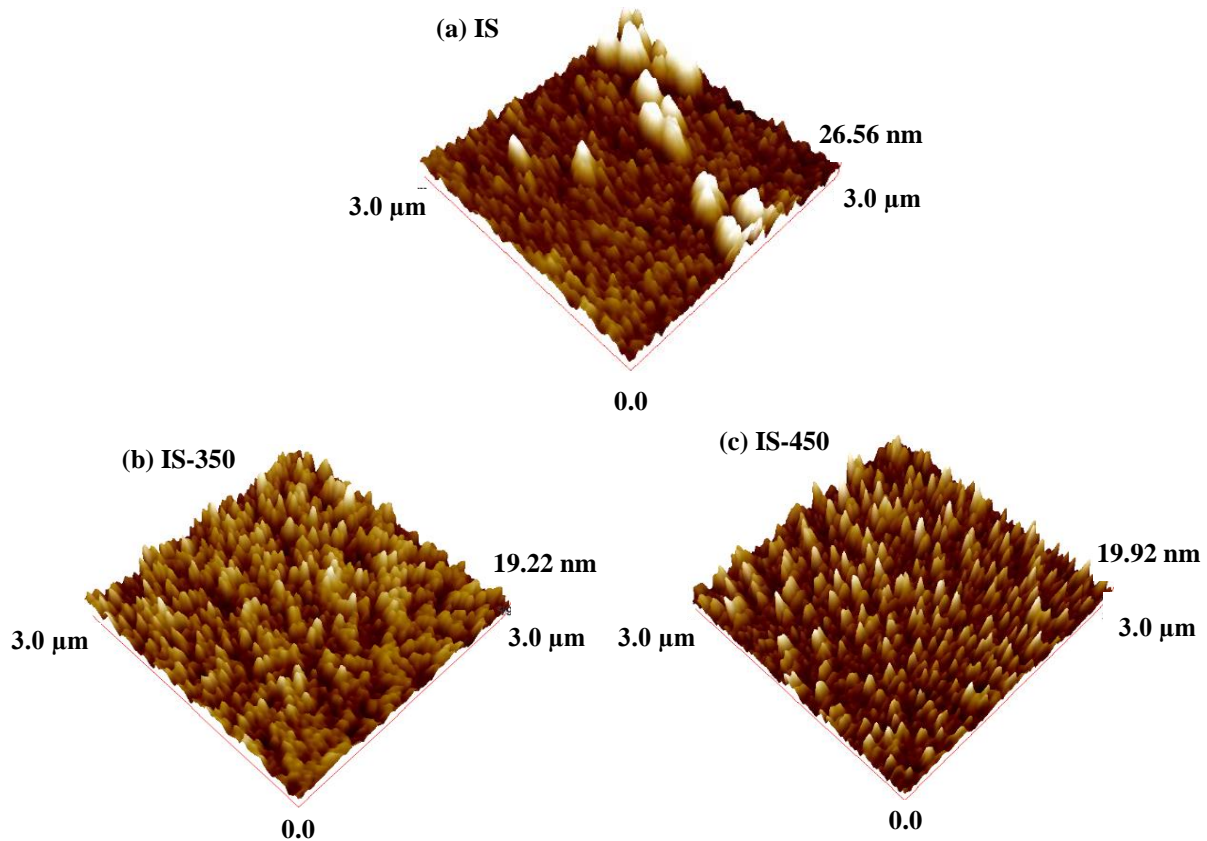


Figure 4. 3D-AFM images of (a) as-deposited, thermally annealed (b) at 350 °C and (c) at 450 °C In_2S_3 films

Table 4. Roughness parameters of the films obtained by AFM analysis

| Sample | R_a (nm) | R_{rms} (nm) | R_t (nm) |
|--------|------------|----------------|------------|
| IS | 2.45 | 3.51 | 26.56 |
| IS-350 | 2.17 | 2.65 | 19.22 |
| IS-450 | 2.24 | 2.87 | 19.92 |

Figure 5 presents the surface and cross-sectional SEM images of the samples IS, IS-350 and IS-450. SEM analysis showed that all films had uniform, homogeneous, and dense surface morphologies without any voids or cracks. From the surface images, it was seen that the sample IS showed a grain growth in granular structure. The post-thermal annealing of the film at 350 °C led to an increase in the compactness of the film. For the samples IS and IS-350, it was observed that some clusters with very small sizes formed on the surfaces. When the temperature raised from 350 °C to 450 °C, the amount, and the sizes of these kinds of clusters on the surface of the film increased. This caused to a surge in the unevenness of the film as perceived in Figure 5 (c), consistent with R_a and R_{rms} values obtained by AFM analysis. The formation of the clusters on the surfaces of the films and the increase in their amounts with thermal annealing treatment can be more clearly seen from SEM cross-sectional images which were taken from a different viewpoint in Figure 6. It was obviously seen that the films consisted of compact grown grains with distinct grain boundaries. The thickness values of the films for the samples IS, IS-350 and IS-450 were determined as 280 nm, 310 nm, and 280 nm from the SEM cross-sectional analysis, respectively. The slight difference in the thickness (~30 nm) of the sample IS-350 can be explained by uneven surface of the SLG substrate and small disparities in the deposition conditions. The thickness values of the films attained through SEM analysis are well agreement with the results obtained by the profilometer measurement.

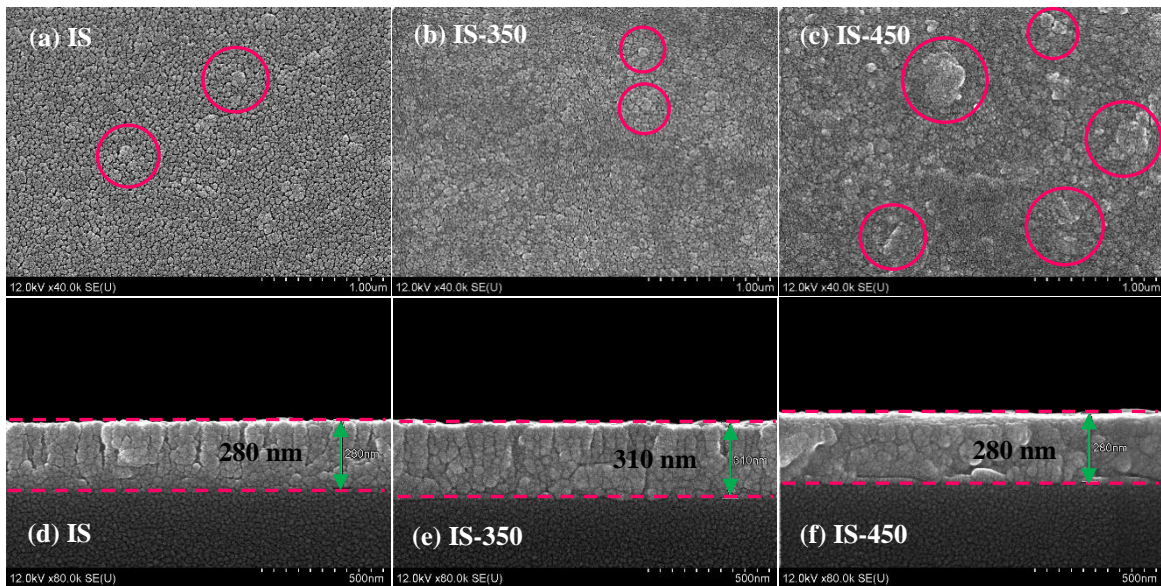


Figure 5. (a)-(c) Surface and (d)-(f) cross-sectional SEM images of the samples IS, IS-350, and IS-450.

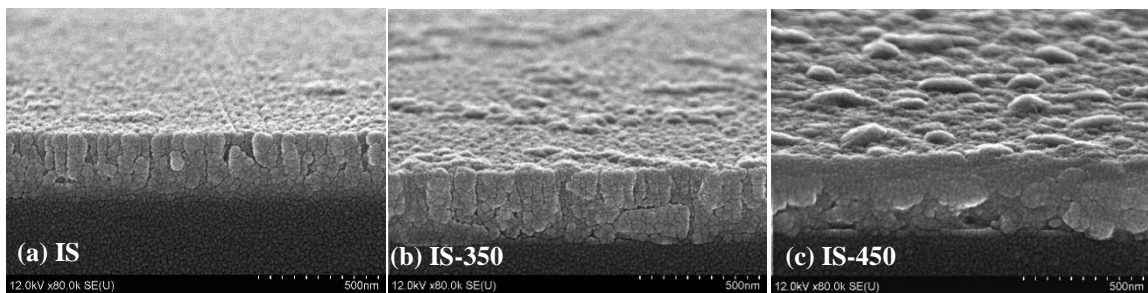


Figure 6. SEM cross-sectional images of the samples (a) IS, (b) IS-350, and (c) IS-450

3.4. Optical Characterization

To understand the optical properties of the prepared and annealed In_2S_3 films, the transmission spectra was recorded from 200 to 1100 nm wavelength range and the obtained results were given in Figure 7(a). The films exhibited average transmissions of 53.34%, 55.27% and 54.53% in the visible region for the samples IS, IS-350 and IS-450, respectively. It was seen that the transmission of the films decreased towards longer wavelengths after reaching a peak point for all samples and then it started to rise again towards the near infrared (NIR) region after about 800 nm. Moreover, the absorption edge got steeper for the sample IS after thermal annealing treatment which can be considered as an indication of improvement in crystallinity of the sample. Although, some studies were previously reported both on reduced and enhanced transmission of the In_2S_3 films with thermal annealing treatment [39, 48, 49], it can be stated that the transmittance spectra of the films in our study were not strongly influenced by the thermal annealing treatment, only small changes were observed. High transparency is desirable for the buffer layers in thin film PVs since it enhances the number of photons in the device. Therefore, our studies on increase of transmission of In_2S_3 films continue taking into account other structural and morphological parameters. Absorption coefficients (α) of the films were calculated from optical transmittance data by using the following equation:

$$\alpha = \frac{1}{d} \ln\left(\frac{1}{T}\right) \quad (5)$$

where d is the thickness of the film and T is the transmittance. The plots of absorption coefficients of the films as a function of photon energy ($h\nu$) were given in Figure 7(b). The absorption coefficients of the films were observed to be in small values in the low photon energy region and increased with the photon energy.

This indicated that the band-to-band transitions took place in the high photon energy region at above 2.1 eV. Similar absorbance spectra were obtained by Guttirez et al. and Nehra et al. [15, 39]. Tauc relation was used to determine the band gap energy values of the as-deposited and thermally annealed films:

$$(\alpha hv)^{1/n} = A(hv - E_g) \quad (6)$$

here, hv - photon energy, E_g - band gap and n is the integer that depends on the nature of the electronic transition which is equal to 1/2 (direct) and 2 (indirect) permissible transitions, respectively.

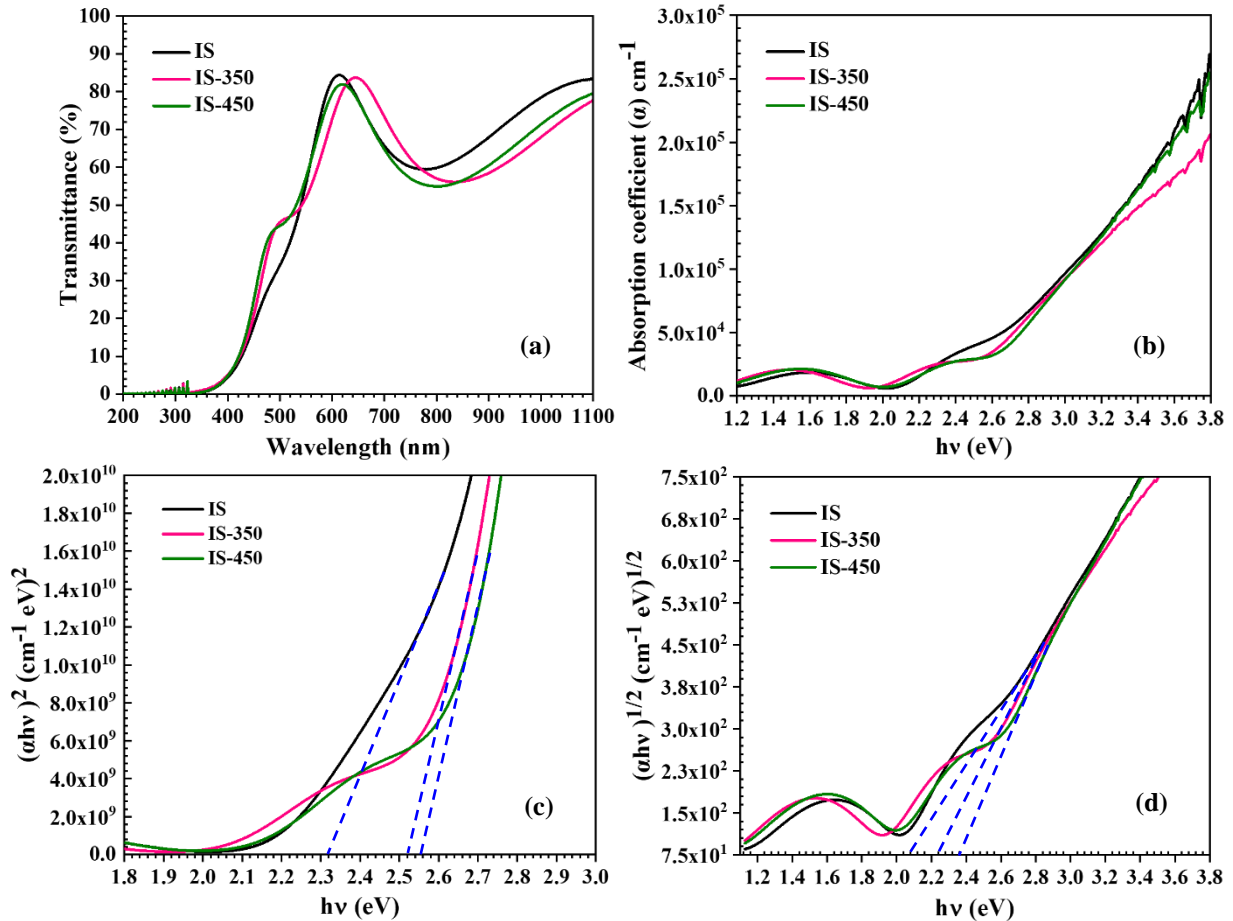


Figure 7. (a) Transmission spectra, (b) the plots of α versus hv , (c) $(\alpha hv)^2$ versus hv (d) $(\alpha hv)^{1/2}$ versus hv of the as-deposited and thermally annealed In_2S_3 films

From Figure 7(c) and 7(d), it was identified that the direct energy band gaps of the films were found as 2.32, 2.52 and 2.56 eV and the indirect energy band gaps of the films were found as 2.08, 2.24 and 2.36 eV, for the samples IS, IS-350 and IS-450, respectively. The observed band gap values were found to be in concordance with the reported band gap values for In_2S_3 films in previous studies [25, 50-52]. Interestingly, it was found that the high temperature treated films had higher E_g than as-deposited films. Kim et al. studied on In_2S_x thin films with various sulfur concentrations and reported that the band gaps of the films shifted towards lower wavelength side (blue shift) with increase in sulfur content [53]. Therefore, it would be more accurate to associate this result with the fact of higher sulfur concentrations of annealed films. From the results of UV-Vis spectroscopy analysis, it can be concluded that the In_2S_3 films grown in this study meet requirements that a buffer layer should have in terms of optical properties for thin film PVs applications, but optical properties can be further improved.

In general, spinel structure $\beta-In_2S_3$ contains high number of defects such as sulfur (V_S : donor) and indium (In) vacancies (V_{In} : acceptor), indium interstitial (In_i : donor) and oxygen in vacancy of sulfur (O_{Vs} : acceptor) [54-56]. In order to have information about the types of the defects existing in the structure, the

films were analyzed by PL spectroscopy at RT. Figure 8(a) shows PL spectra of the as-deposited and thermally annealed In_2S_3 films. In the spectra of the films, three broad emission bands were observed at around 1.70, 2.20 and 2.71 eV. It is known that the oxygen replaces Vs site in In_2S_3 and creates an acceptor level at around 0.82-0.88 eV above the valance band [57]. Therefore, the red emissions (P1) at around 1.70 eV in our study were attributed to radiative transitions from indium interstitial (In_i) donors to oxygen in vacancy of sulfur (O_{Vs}) acceptors [58-60]. The intensity of the red emission showed a remarkable increase with the thermal annealing process at 350 °C and it decreased again with the thermal annealing process at 450 °C. This confirmed better crystalline, morphological, and optical properties of the sample IS-450 obtained by XRD and AFM analysis. The green emissions (P2) centered at around 2.20 eV were attributed to transitions from V_S donor states to V_In acceptor states [49, 59, 60].

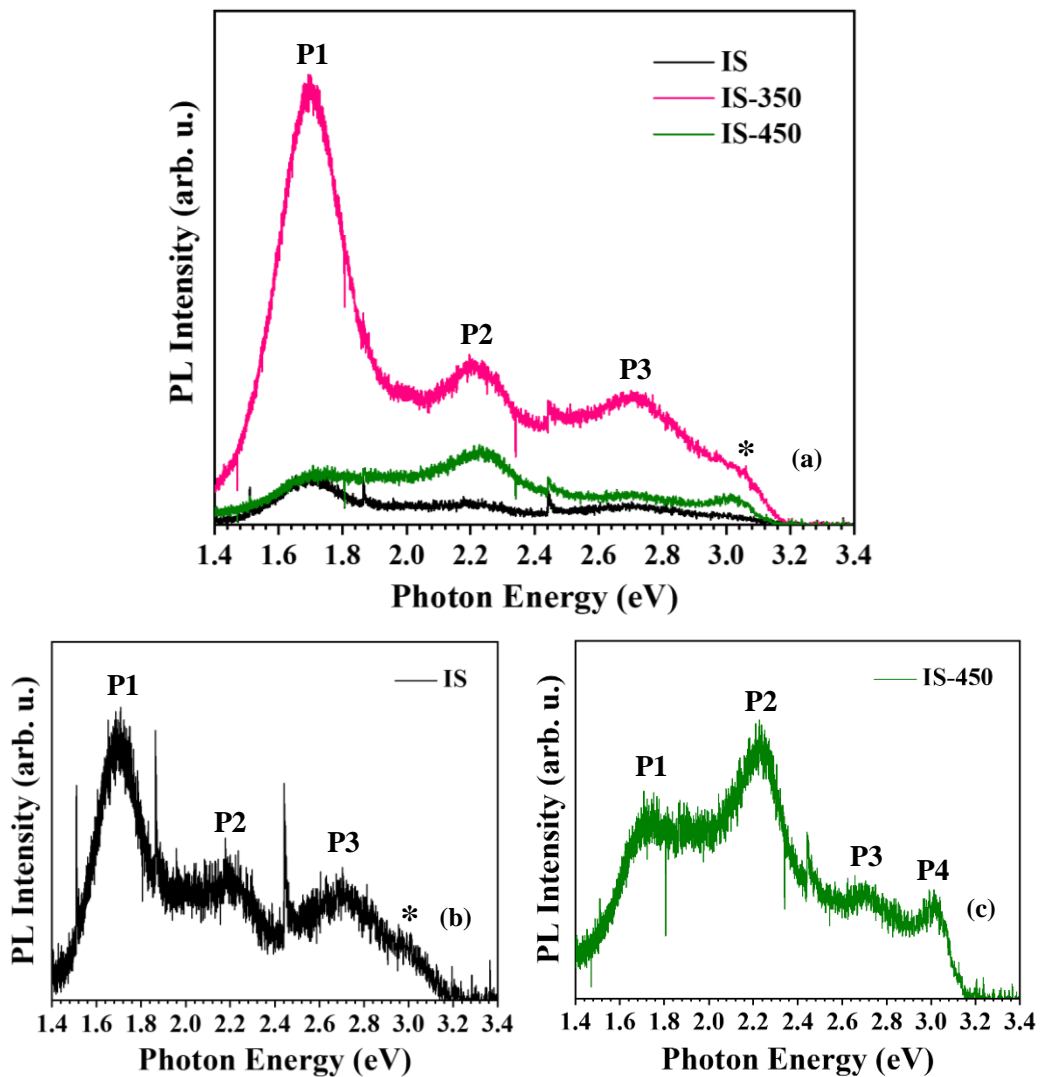


Figure 8. RT-PL spectra of (a) as-deposited and thermally annealed In_2S_3 films, the PL spectra of (b) the sample IS, and (c) the sample IS-450 separately

The third emissions (P3) at around 2.71 eV in the blue light region can be associated with the recombination of the electrons occupying the sulfur vacancies with photo-excited holes or to the PL emission resulting from $\beta\text{-In}_2\text{S}_{3-3x}\text{O}_{3x}$ due to the oxidation of the surfaces of the films [49, 56, 61]. Another blue emission peak (P4) was observed at around 3.03 eV for the sample IS-450. This peak was observed as a shoulder (marked by asterisk in Figure 8(a) and (b)) which is accompanying with the P3 emission peak for the samples IS and IS-350. Souli et al. and Bensalem et al. also observed such a blue emission peak in their study and they reported that this peak was probably because of defect level related to interface traps at grain boundaries and thus, the transitions between this level and valance band [62, 63]. To better evaluation the PL intensities

of the films, the PL spectrum of the sample IS and IS-450 were also given separately in Figure 8(b) and (c). It is concluded that there were no significant changes in the peak positions after the as-deposited films were annealed at 350 °C and 450°C, and thermal annealing process changed the densities of the luminescence centers, and this caused to a change in the PL emission intensities.

4. CONCLUSION

The In₂S₃ thin films with the thickness of 280 nm were deposited on SLG by RF magnetron sputtering technique and the effect of the thermal annealing treatment at 350 °C and 450 °C were investigated. XRD and AFM results displayed that the crystallization and topographical morphology of the films enhanced with thermal annealing treatment at 450 °C and it was determined that these films had slightly sulfur deficit composition. It is inferred from the cross-sectional SEM analysis that the films consisted of compact grown grains with distinct grain boundaries. The films showed an average transmission in the range of 53% - 55% in the visible region. From optical analysis, it was demonstrated the existence of direct and indirect allowed transitions. It is important to indicate here that the band gaps of the as-deposited films increased with the thermal annealing process. With an increase of the annealing temperature from 350 °C to 450 °C, the energy band gaps increased from 2.52 eV to 2.56 eV and from 2.24 eV to 2.36 eV for the direct and indirect allowed transitions, respectively. In the RT-PL spectra, two strong and broad emission bands were observed at around 1.70 eV and 2.20 eV corresponding to the transitions from In_i donors to O_{Vs} acceptors and from V_S donor states to V_{In} acceptor states, respectively. In addition, the emissions at around 2.71 eV and 3.03 eV in the blue light region were attributed to the emission resulting from β-In₂S_{3-3x}O_{3x} due to the oxidation of the surfaces of the films and the transitions between defect level related to interface traps at grain boundaries and valance band, respectively. As a result, the temperature value of 450 °C can be considered as a suitable temperature for the thermal annealing treatment of the as-deposited RF-sputtered In₂S₃ thin films to improve their structural, morphological, and optical properties.

ACKNOWLEDGMENTS

This work was supported by Presidency of Turkey, Presidency of Strategy and Budget with 2016K121220 project number, TUBITAK with the grant № 118F009 and by the Belarusian State Programme for Research «Physical material science, new materials, and technologies».

CONFLICTS OF INTEREST

No conflict of interest was declared by the authors.

REFERENCES

- [1] Shockley, W., Queisser H.J., “Detailed balance limit of efficiency of p-n junction solar cells”, *Journal of Applied Physics*, 32(3): 510-519, (1961).
- [2] Green, M.A., Dunlop, E.D., Hohl-Ebinger, J., Yoshita, M., Kopidakis, N., Hao, X., “Solar cell efficiency tables (version 59)”, *Progress in Photovoltaics: Research and Applications*, 30: 3-12, (2022).
- [3] Wilson, G., Al-Jassim, M.M., Metzger, W., Glunz, S.W., Verlinden, P., Gang, X., Mansfield, L., Stanbery, B.J., Zhu, K., Yan, Y. “The 2020 Photovoltaic Technologies Roadmap”, *Journal of Physics D: Applied Physics*, 53(49): 493001, (2020).
- [4] Mufti, N., Amrillah, T., Taufiq, A., Diantoro, M., Nur, H., “Review of CIGS-based solar cells manufacturing by structural engineering”, *Solar Energy*, 207: 1146-1157, (2020).
- [5] Sinha, T., Lilhare, D., Khare, A., “A review on the improvement in performance of CdTe/CdS thin-film solar cells through optimization of structural parameters”, *Journal of Materials Science*, 54(19): 12189-12205, (2019).

- [6] Prabeesh, P., Sajeesh, V., Selvam, I.P., Bharati, M.D., Rao, G.M., Potty, S., "CZTS solar cell with non-toxic buffer layer: A study on the sulphurization temperature and absorber layer thickness", *Solar Energy*, 207: 419-427, (2020).
- [7] Kowsar, A., Farhad, S.F.U., Rahaman, M., Islam, M.S., Imam, A.Y., Debnath, S.C., Sultana, M., Hoque, M.A., Sharmin, A., Mahmood, Z.H., "Progress in major thin-film solar cells: Growth technologies, layer materials and efficiencies", *International Journal of Renewable Energy Research*, 9(2): 579-597, (2019).
- [8] Kato, T., Wu, J.-L., Hirai, Y., Sugimoto, H., Bermudez, V., "Record efficiency for thin-film polycrystalline solar cells up to 22.9% achieved by Cs-treated Cu(In, Ga)(Se, S)₂", *IEEE Journal of Photovoltaics*, 9(1): 325-330, (2018).
- [9] PV Magazine, First Solar raises bar for CdTe with 21.5% efficiency record, (2015).
- [10] Yan, C., Huang, J., Sun, K., Johnston, S., Zhang, Y., Sun, H., Pu, A., He, M., Liu, F., Eder, K. "Cu₂ZnSnS₄ solar cells with over 10% power conversion efficiency enabled by heterojunction heat treatment", *Nature Energy*, 3(9): 764-772, (2018).
- [11] Tao, J., Liu, J., Chen, L., Cao, H., Meng, X., Zhang, Y., Zhang, C., Sun, L., Yang, P., Chu, J., "7.1% efficient co-electroplated Cu₂ZnSnS₄ thin film solar cells with sputtered CdS buffer layers", *Green Chemistry*, 18(2): 550-557, (2016).
- [12] Kogler, W., Schnabel, T., Ahlswede, E., Taskesen, T., Gütay, L., Hauschild, D., Weinhardt, L., Heske, C., Seeger, J. Hetterich, M., "Hybrid chemical bath deposition-CdS/sputter-Zn(O, S) alternative buffer for Cu₂ZnSn(S, Se)₄ based solar cells", *Journal of Applied Physics*, 127(16): 165301, (2020).
- [13] Jiang, F., Ozaki, C., Harada, T., Tang, Z., Minemoto, T., Nose, Y., and Ikeda, S., "Effect of indium doping on surface optoelectrical properties of Cu₂ZnSnS₄ photoabsorber and interfacial/photovoltaic performance of cadmium free In₂S₃/Cu₂ZnSnS₄ heterojunction thin film solar cell", *Chemistry of Materials*, 28(10): 3283-3291, (2016).
- [14] Chantana, J., Kato, T., Sugimoto, H., and Minemoto, T., "Heterointerface recombination of Cu(In, Ga)(S, Se)₂-based solar cells with different buffer layers", *Progress in Photovoltaics: Research and Applications*, 26(2): 127-134, (2018).
- [15] Galarza Gutiérrez, U., de Albor Aguilera, M.L., Hernández Vasquez, C., Flores Márquez, J.M., González Trujillo, M.A., Jiménez Olarte, D., Aguilar Hernández, J.R., Remolina Millán, A., "Structural and Optoelectronic Properties of β-In₂S₃ Thin Films to be Applied on Cadmium Reduced Solar Cells", *physica status solidi (a)*, 215(4): 1700428, (2018).
- [16] Mughal, M.A., Engelken, R., Sharma, R., "Progress in indium (III) sulfide (In₂S₃) buffer layer deposition techniques for CIS, CIGS, and CdTe-based thin film solar cells", *Solar Energy*, 120: 131-146, (2015).
- [17] Soni, P., Raghuvanshi, M., Wuerz, R., Berghoff, B., Knoch, J., Raabe, D., Cojocaru-Mirédin, O., "Sputtering as a viable route for In₂S₃ buffer layer deposition in high efficiency Cu(In, Ga)Se₂ solar cells", *Energy Science & Engineering*, 7(2): 478-487, (2019).
- [18] Pistor, P., Merino Álvarez, J.M., León, M., Di Michiel, M., Schorr, S., Klenk, R., Lehmann, S., "Structure reinvestigation of α-, β-and γ-In₂S₃", *Acta Crystallographica Section B: Structural Science, Crystal Engineering and Materials*, 72(3): 410-415, (2016).
- [19] Rasool, S., Saritha, K.R. Reddy, K., Tivanov, M., Trofimova, A., Tikoto, S., Bychto, L., Patryn, A., Maliński, M., Gremenok, V., "Effect of annealing on the physical properties of thermally evaporated In₂S₃ thin films", *Current Applied Physics*, 19: 108-113, (2019).

- [20] Stumph, P., Baranova, K., Rogovoy, M., Bunakov, V., Maraeva, E., Tulenin, S., "Chemical bath deposition of In_2S_3 thin films as promising material and buffer layer for solar cells", AIP Conference Proceedings AIP Publishing LLC, 2063(1): 040057, (2019).
- [21] Souissi, R., Bouguila, N., Bendahan, M., Fiorido, T., Aguir, K., Kraini, M., Vázquez-Vázquez, C., Labidi, A., "Highly sensitive nitrogen dioxide gas sensors based on sprayed $\beta\text{-In}_2\text{S}_3$ film", Sensors and Actuators B: Chemical, 319: 128280, (2020).
- [22] Sterner, J., Malmström, J., Stolt, L., "Study on ALD $\text{In}_2\text{S}_3/\text{Cu}$ (In, Ga) Se_2 interface formation", Progress in Photovoltaics: Research and Applications, 13(3): 179-193, (2005).
- [23] Mughal, M.A., Alqudsi, A., Rao, P.M., Masroor, M., Ichwani, R., Zhou, L., Giri, B., "All-electrodeposited p- $\text{Cu}_2\text{ZnSnS}_4/n\text{-In}_2\text{S}_3$ Heterojunction Formation for Solar Cell Applications", 2018 IEEE 7th World Conference on Photovoltaic Energy Conversion (WCPEC) (A Joint Conference of 45th IEEE PVSC, 28th PVSEC & 34th EU PVSEC) IEEE, 142-147, (2018).
- [24] Karthikeyan, S., Hill, A.E., Pilkington, R.D., "Low temperature pulsed direct current magnetron sputtering technique for single phase $\beta\text{-In}_2\text{S}_3$ buffer layers for solar cell applications", Applied Surface Science, 418: 199-206, (2017).
- [25] Ji, Y., Ou, Y., Yu, Z., Yan, Y., Wang, D., Yan, C., Liu, L., Zhang, Y., Zhao, Y., "Effect of film thickness on physical properties of RF sputtered In_2S_3 layers", Surface and Coatings Technology, 276: 587-594, (2015).
- [26] Spiering, S., Nowitzki, A., Kessler, F., Igalson, M., Maksoud, H.A., "Optimization of buffer-window layer system for CIGS thin film devices with indium sulphide buffer by in-line evaporation", Solar Energy Materials and Solar Cells, 144: 544-550, (2016).
- [27] Kim, J., Hiroi, H., Todorov, T.K., Gunawan, O., Kuwahara, M., Gokmen, T., Nair, D., Hopstaken, M., Shin, B., Lee, Y.S., "High efficiency Cu_2ZnSn (S, Se) $_4$ solar cells by applying a double $\text{In}_2\text{S}_3/\text{CdS}$ emitter", Advanced Materials, 26(44): 7427-7431, (2014).
- [28] Hariskos, D., Spiering, S., Powalla, M., "Buffer layers in Cu (In, Ga) Se_2 solar cells and modules", Thin Solid Films, 480: 99-109, (2005).
- [29] Abou-Ras, D., Kostorz, G., Hariskos, D., Menner, R., Powalla, M., Schorr, S., Tiwari, A., "Structural and chemical analyses of sputtered In_xS_y buffer layers in Cu (In, Ga) Se_2 thin-film solar cells", Thin Solid Films, 517(8): 2792-2798, (2009).
- [30] Hariskos, D., Hempel, W., Menner, R., Witte, W., "Influence of Substrate Temperature during In_xS_y Sputtering on Cu (In, Ga) Se_2 /Buffer Interface Properties and Solar Cell Performance", Applied Sciences, 10(3): 1052, (2020).
- [31] Wang, S., Shiou, F., Tsao, C., Huang, S., Hsu, C., "An evaluation of the deposition parameters for indium sulfide (In_2S_3) thin films using the grey-based Taguchi method", Materials Science in Semiconductor Processing, 16: 1879-1887, (2013).
- [32] Hwang, D.H., Cho, S., Hui, K.N., Son, Y.G., "Effect of sputtering power on structural and optical properties of radio frequency-sputtered In_2S_3 thin films", Journal of Nanoscience and Nanotechnology, 14: 8978-8981, (2014).
- [33] Siol, S., Dhakal, T.P., Gudavalli, G.S., Rajbhandari, P.P., DeHart, C., Baranowski, L.L., and Zakutayev, A., "Combinatorial reactive sputtering of In_2S_3 as an alternative contact layer for thin film solar cells", Acs Applied Materials & Interfaces, 8: 14004-14011, (2016).
- [34] Soni, P., Raghuvanshi, M., Wuerz, R., Berghoff, B., Knoch, J., Raabe, D., Cojocar-Mirédin, O., "Role of elemental intermixing at the $\text{In}_2\text{S}_3/\text{CIGSe}$ heterojunction deposited using reactive RF magnetron sputtering", Solar Energy Materials & Solar Cells, 195: 367-375, (2019).

- [35] Gremenok, V.F., Ramakrishna Reddy, K., Tivanov, M.S., Patryn, A., “Effect of annealing on the Structure of thermal evaporated In_2S_3 thin films”, *Przegląd Elektrotechniczny*, 93: 89-91, (2017).
- [36] Sandoval-Paz, M., Sotelo-Lerma, M., Valenzuela-Jauregui, J., Flores-Acosta, M., Ramirez-Bon, R., “Structural and optical studies on thermal-annealed In_2S_3 films prepared by the chemical bath deposition technique”, *Thin Solid Films*, 472: 5-10, (2005).
- [37] Rasool, S., Saritha, K., Reddy, K.R., Bychto, L., Patryn, A., Maliński, M., Tivanov, M., Gremenok, V., “Optoelectronic properties of In_2S_3 thin films measured using surface photovoltage spectroscopy”, *Materials Research Express*, 6: 076417, (2019).
- [38] Timoumi, A., Bouzouita, H., Brini, R., Kanzari, M., Rezig, B., “Optimization of annealing conditions of In_2S_3 thin films deposited by vacuum thermal evaporation”, *Applied Surface Science*, 253: 306-310, (2006).
- [39] Nehra, S., Chander, S., Sharma, A., Dhaka, M., “Effect of thermal annealing on physical properties of vacuum evaporated In_2S_3 buffer layer for eco-friendly photovoltaic applications”, *Materials Science Semiconductor Processing*, 40: 26-34, (2015).
- [40] Rietveld, H.M., “A profile refinement method for nuclear and magnetic structures”, *Journal of Applied Crystallography*, 2(2): 65-71, (1969).
- [41] Lutterotti, L., Matthies, S. and Wenk, H.-R., “MAUD (material analysis using diffraction): a user friendly Java program for Rietveld texture analysis and more”, *Proceeding of the twelfth international conference on textures of materials, (ICOTOM-12) NRC Research Press Ottawa, Canada*, 1: 1599, (1999).
- [42] Cullity, B.D., Stock, S.R., “Elements of X-Ray Diffraction”, Third Edition, Pearson, U.K., (2014).
- [43] Tiss, B., Erouel, M., Bouguila, N., Kraini, M., and Khirouni, K., “Effect of silver doping on structural and optical properties of In_2S_3 thin films fabricated by chemical pyrolysis”, *Journal of Alloys and Compounds*, 771: 60-66, (2019).
- [44] Williamson, G., Smallman, R., III. “Dislocation densities in some annealed and cold-worked metals from measurements on the X-ray debye-scherrer spectrum”, *Philosophical Magazine*, 1: 34, (1956).
- [45] Thanikaikarasan, S., “Role of electrolyte concentration on growth kinetics, film thickness, structural, compositional and optical properties of cadmoselite thin films through electrochemical route”, *Journal of Alloys and Compounds*, 885: 160963, (2021).
- [46] Mahmood, W., Ali, J., Zahid, I., Thomas, A., ul Haq, A., “Optical and electrical studies of CdS thin films with thickness variation”, *Optik*, 158: 1558-1566, (2018).
- [47] Kumar, B.H., Kumar, M.S., “On the conversion of amorphous In_2S_3 thin films to polycrystalline In_2S_3 and to In_2O_3 through thermal oxidation process”, *Materials Science in Semiconductor Processing*, 111: 104983, (2020).
- [48] Rao, P., Kumar, S., “Growth of stoichiometric indium sulfide films by thermal evaporation: Influence of vacuum annealing on structural and physical properties”, *Thin Solid Films*, 524: 93-99, (2012).
- [49] Assili, K., Selmi, W., Alouani, K., Vilanova, X., “Computational study and characteristics of In_2S_3 thin films: effects of substrate nature and deposition temperature”, *Semiconductor Science and Technology*, 34(4): 045006, (2019).
- [50] Lugo-Loredo, S., Peña-Méndez, Y., Calixto-Rodríguez, M., Messina-Fernández, S., Alvarez-Gallegos, A., Vázquez-Dimas, A. and Hernández-García, T., “Indium sulfide thin films as window layer in chemically deposited solar cells”, *Thin Solid Films*, 550: 110-113, (2014).

- [51] Tivanov, M., Svito, I., Rasool, S., Saritha, K., Reddy, K.R., Gremenok, V., "Effect of heat treatment in sulfur on structural, optical and electrical properties of thermally evaporated In_2S_3 thin films", *Solar Energy*, 222: 290-297, (2021).
- [52] Hashemi, M., Minbashi, M., Ghorashi, S.M.B., Ghobadi, A., "A modeling study on utilizing low temperature sprayed In_2S_3 as the buffer layer of CuBaSn(S, Se) solar cells", *Scientific Reports*, 11(1): 1-11, (2021).
- [53] Kim, W.T., Kim, C.D., "Optical energy gaps of $\beta\text{-In}_2\text{S}_3$ thin films grown by spray pyrolysis", *Journal of Applied Physics*, 60(7): 2631-2633, (1986).
- [54] Ho, C.H., "Growth and characterization of near-band-edge transitions in $\beta\text{-In}_2\text{S}_3$ single crystals", *Journal of Crystal Growth*, 312(19): 2718-2723, (2010).
- [55] Kraini, M., Bouguila, N., Halidou, I., Moadhen, A., Vázquez-Vázquez, C., López-Quintela, M., Alaya, S., "Study of optical and electrical properties of In_2S_3 : Sn films deposited by spray pyrolysis", *Journal of Electronic Materials*, 44(7): 2536-2543, (2015).
- [56] Ho, C.-H., Lin, M.-H., Wang, Y.-P., Huang, Y.-S., "Synthesis of In_2S_3 and Ga_2S_3 crystals for oxygen sensing and UV photodetection", *Sensors and Actuators A: Physical*, 245: 119-126, (2016).
- [57] Jayakrishnan, R., "Photoluminescence in Spray Pyrolysis Deposited $\beta\text{-In}_2\text{S}_3$ Thin Films", *Journal of Electronic Materials*, 47(4): 2249-2256, (2018).
- [58] Jayakrishnan, R., John, T.T., Kartha, C.S., Vijayakumar, K., Jain, D., Chandra, L.S., Ganesan, V., "Do the grain boundaries of $\beta\text{-In}_2\text{S}_3$ thin films have a role in sub-band-gap photosensitivity to 632.8 nm?", *Journal of Applied Physics*, 103(5): 053106, (2008).
- [59] Rajeshmon, V., Poornima. N., Kartha, C.S., Vijayakumar, K., "Modification of the optoelectronic properties of sprayed In_2S_3 thin films by indium diffusion for application as buffer layer in CZTS based solar cell", *Journal of Alloys and Compounds*, 553: 239-244, (2013).
- [60] Jayakrishnan, R., Sebastian, T., Sudha Kartha, C., Vijayakumar, K., "Effect of defect bands in $\beta\text{-In}_2\text{S}_3$ thin films", *Journal of Applied Physics*, 111(9): 093714, (2012).
- [61] Cao, G., Zhao, Y., Wu, Z., "Synthesis and characterization of In_2S_3 nanoparticles", *Journal of Alloys and Compounds*, 472(1-2): 325-327, (2009).
- [62] Salem, Y.B., Kilani, M., Kamoun, N., "Effect of deposition runs on the physical properties of In_2S_3 chemically synthesized for photocatalytic application", *Results in Physics*, 10: 706-713, (2018).
- [63] Souli, M., Bensalem. Y., Secu, M., Bartha, C., Enculescu, M., Mejri, A., Kamoun-Turki, N., Badica, P., "Effect of high gamma radiations on physical properties of In_2S_3 thin films grown by chemical bath deposition for buffer layer applications", *Results in Physics*, 13: 102115, (2019).